Journal of Materials Chemistry A

Accepted Manuscript

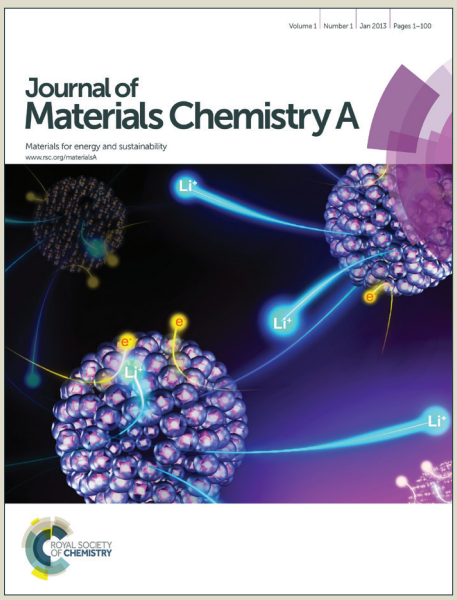

ROYAL SOCIETY OF CHEMISTRY

www.rsc.org/materialsA

Journal of Materials Chemistry

Dynamic Article Links ►

Cite this: DOI: 10.1039/c0xx00000x

www.rsc.org/materials

ARTICLE TYPE

A novel MOF/graphene oxide composite GrO@MIL-101 with high adsorption capacity of acetone

Xin Zhou, Wenyu Huang, Jiao Shi, Zhenxia Zhao, Qibin Xia, Yingwei Li, Haihui Wang, Zhong Li*

Received (in XXX, XXX) Xth XXXXXXXXX 20XX, Accepted Xth XXXXXXXXX 20XX

DOI: 10.1039/b000000x

ABSTRACT: A novel composite material GrO@MIL-101 was synthesized using a solvothermal synthesis method. Then the parent materials (MIL-101 and graphene oxide) and the GrO@MIL-101 were characterized using SEM, TEM, XRD, nitrogen sorption, and Raman. The acetone isotherms on the GrO@MIL-101 and MIL-101 were measured separately. The isosteric heat of adsorption and the desorption activation energies of acetone on the two samples were estimated. The results of characterization confirmed the formation of well-defined GrO@MIL-101 with higher surface area and pore volume compared to the MIL-101, and the crystal size of the MIL-101 in the composite were smaller than that of the parent MIL-101. The acetone isotherms on the GrO@MIL-101 were much higher than the MIL-101. The acetone adsorption capacity of the GrO@MIL-101 was up to 20.10 mmol g^{-1} at 288K and 161.8 mbar, having an increase of 44.4% in comparison with the MIL-101. The desorption activation energy of acetone on the GrO@MIL-101 were higher than that on the MIL-101, indicating the stronger interaction between acetone molecules and the GrO@MIL-101. Consecutive cycles of acetone adsorption-desorption showed that the desorption efficiency of acetone on the GrO@MIL-101 can reach 91.3%. Acetone adsorption on this composite material was highly reversible.

CREATED USING THE RSC ARTICLE TEMPLATE (VER. 3.0) - SEE WWW.RSC.ORG/ELECTRONICFILES FOR DETAILS

ARTICLE TYPE www.rsc.org/xxxxxx | XXXXXXXX

1 Introduction

Metal organic frameworks (MOFs) are a novel class of crystalline porous materials, and have recently attracted intense research interest because of their ultrahigh specific area, well-defined framework structures, tuneable functionalities, and potential applications in the fields of gas storage, separation and purification.[1-4] In the past two decades, we have witnessed an explosion in the research and development of new porous materials, the spearhead being porous MOFs.[5, 6] Nevertheless, it was noticed that although MOFs have ultrahigh specific area, their low density of atoms in structure cannot provide dispersive forces strong enough to bind small molecules.[7, 8] In other words, there are spaces to improve the adsorption performance of MOFs by means of compositing the MOFs and graphitic components (graphite oxide or graphene oxide) or chemical modification of surfaces. In recent years, increasing efforts are being put forth to improve the performance of the MOFs so as to ensure the potential applications of MOFs.

Petit et al. synthesized the MOF-5/GO composite by using a solvothermal synthesis route, and then tested its adsorption capacity as ammonia adsorbent.[9] It was found that the prepared composite material had a unique layered texture with a preserved structure of MOF-5 and GO, and showed some synergy enhancing the adsorption capacity in comparison with the hypothetical physical mixture of the components. Bandosz et al. prepared two types of MOF/graphite oxide hybrid materials.[10] One was based on a zinc-containing, MOF-5 and the other on a copper-containing HKUST-1. It was found that these composite compounds exhibited similar features in crystalline structure and porosity to the parent MOFs, and their ammonia adsorption capacity became higher compared to their parent MOFs due to creation of new pores between the two phases MOF units and GO. Levasseur et al. synthesized composites of HKUST-1 and GO, and studied its reactive adsorption of NO_2 in dry and moist conditions.[11] They reported that in dry conditions, the composites exhibited higher NO_2 breakthrough capacity compared to MOF and GO due to the increased porosity and the reactive adsorption of NO_2 on copper. Bandosz and her coworkers tried to synthesize composites of MIL-100(Fe) and GO with various ratios of the two components, and then tested for ammonia removal in dynamic conditions.[12] Unfortunately, the formation of well-defined MIL-100(Fe)/GO composites was not favoured due to limit of the specific geometry of MIL-100(Fe). The authors thought that the spherical pores of MIL-100(Fe) led to various possible coordination orientations between GO and MIL units, and thus affected the formation of the whole framework. MIL-101 is one of the most porous materials to date, being a very prominent adsorbent among the many MOFs that have been studied. It has very large Langmuir surface area (~5900 ± 300 m^2 g^{-1}) and huge cell volume (~702000 $Å^3$) with two types of quasi-spherical cages limited by 12 pentagonal faces for the smaller and by 16 faces (12 pentagonal and 4 hexagonal) for larger.[13] However, composite of graphene oxide (GrO) and MIL-101 has not been reported yet. If GO was exfoliated into GrO with fewer layers, the formation of well-defined MIL/GO framework will be more favoured. Therefore, a novel composite GrO@MIL-101 is worthy of studying.

The objective of this work is to investigate a novel composite GrO@MIL-101 for enhancement of adsorption toward acetone. The composite GrO@MIL-101 was firstly synthesized and then characterized. Its features are compared to the parent materials. Acetone would be chosen as probe molecule to study adsorption performance of the composite since it is not only a model molecule representing a category of small polar molecules, but also widely used as organic solvent which has caused air pollution in many occasions. Temperature programmed desorption (TPD) experiments were conducted to estimate the desorption activation energy of acetone on the GrO@MIL-101 and MIL-101. Consecutive adsorption-desorption cycles were also performed to examine the reversibility of acetone adsorption on these two materials.

2 Experimental

2.1 Materials and Methods: All chemicals were of reagent-grade quality obtained from commercial sources and used without further purification. MIL-101 and GrO were synthesized according to the literature with modification.

2.2 Synthesis of MIL-101: The chromium terephthalate MIL-101 was synthesized via hydrothermal method, and the original steps were already reported elsewhere [13]. Firstly, the reactant mixture with a molar composition of 1 $Cr(NO_3)_3$•$9H_2O$: 1 H_2BDC : 1 HF : 278 H_2O was loaded into a Teflon-lined stainless steel reactor and then sealed. Secondly, the reactor was placed in an autoclave (CWF 1300, Carnolite) at 493 K and held for 8 h. Then, the reactor was gradually cooled down to the room temperature. Fine green powders were obtained as the major product, while a significant amount of recrystallized H_2BDC could be found. To acquire pure crystalline material with high porosity and surface area, a series of purification were applied to remove the unreacted H_2BDC as well as other guest molecules in the sample. The procedure of purification was mainly comprised with two consecutive solvent treatments using N,N-dimethylformamide and hot ethanol solution separately. After that, the product was dried at 423 K overnight. Finally, the crystalline material of MIL-101 was obtained.

2.3 Synthesis of GrO: Graphite oxide was prepared by oxidation of graphite powder via modified Hummers' method[14, 15]. Firstly, Graphite powder (4 g) and sodium nitrate (4 g) were added into concentrated sulfuric acid (200 mL) stirred in ice bath. Then, potassium permanganate (24 g) was slowly added to the suspension at temperature below 293 K. The suspension was stirred for 30 minutes in ice bath. The stirring went on for the next 48 hours at room temperature. Distilled water (368 mL) was slowly added in 15 minutes, and then the suspension was further diluted with warm distilled water (1120 mL). Hydrogen peroxide (80 mL) was added and the mixture was left overnight. Graphite oxide particles were separated by centrifugation before washed by deionized water to eliminate acid. After that, the particles were

Journal of Materials Chemistry

Dynamic Article Links ►

Cite this: DOI: 10.1039/c0xx00000x

www.rsc.org/materials

ARTICLE TYPE

dried at 333 K in vacuum for 36 hours. Finally, the graphite oxide particles were exfoliated and partially reduced at 623 K in nitrogen atmosphere for several minutes, and thus the desired graphene oxide were obtained, which was labelled as GrO.

2.4 Synthesis of GrO@MIL-101: The composite material GrO@MIL-101 was prepared by using a similar method employed in Synthesis of MIL-101. Firstly the reactant mixture with a molar composition of 1 $Cr(NO_3)_3$•$9H_2O$: 1 H_2BDC : 1 HF : 278 H_2O was well-dissolved, and then GrO was added into the mixture with a mass composition of 1 GrO: 10 $Cr(NO_3)_3$•$9H_2O$. Secondly, the resulting suspension was sonicated for 30 minutes, and stirred at 313 K for another 15 minutes. After that, the suspension was transferred into an oven, and then headed at 493K for 8 hours, followed by a two-step purification in which N,N-dimethylformamide and hot ethanol were used separately to remove the residual of H_2BDC. Finally, the product was dried at 423 K for 12 hours and thus the GrO@MIL-101 was obtained.

2.5 Adsorbent Characterization: The surface morphology of the samples was observed by using a Philips FEI XL-30 scanning electron microscope (SEM) after gold deposition. Transmission electron microscope (TEM) was performed on JEOL JEM-2010HR after the samples were suspended in ethanol. XRD measurements were performed on the D/max-IIIA diffractometer (Rigaku Co.) with Cu Kα1 radiation (λ=1.54056). The surface organic FTIR spectroscopy was carried out using a Bruker 550 FTIR instrument equipped with a diffuse reflectance accessory that including a reaction cell. The samples were outgassed at 423K for 5 hours and then mixed with KBr powder. The sample chamber was kept purged with nitrogen during the entire experiment. Data acquisition was performed automatically using a commercial software package. The spectra were collected in the range of 400–2000 cm^{-1} with a resolution of 4 cm^{-1}. Raman spectroscopy was carried out by using a Horiba Jobin-Yvon ARAMIS Raman apparatus with a He-Ne laser (λ = 632.8 nm). The laser power was controlled below 0.1 mW to avoid laser-induced local heating. A 50 objective lens was used in Raman experiment and the spectra resolution was 1 cm^{-1}. Nitrogen isotherms were measured at 77 K on the Micromeritics ASAP 2010 equipped with commercial software of calculation and analysis. The samples were outgassed at 423K for 5 hours before measurement. The pore textural properties including specific Langmuir and BET surface area, pore size and pore volume can obtained by analyzing the N_2 adsorption/desorption isotherms. The elemental analysis of Cr was performed on the IRIS (HR) inductively coupled plasma-atomic emission spectrometry (ICP-AES) (Thermo Jarrell Ash Co.) to calculate the GrO content of the GrO@MIL-101.

2.6 Acetone Vapour Adsorption Experiments: The intelligent gravimetric analyzer (IGA-003, Hiden) was employed to perform the acetone adsorption experiments. The samples were outgassed at 423 K for 5 hours in vacuum before each measurement, and the measurements were performed at 288 K, 298 K, 308 K and 318 K respectively.

2.7 Temperature Programmed Desorption Experiments: The temperature programmed desorption (TPD) experiments were carried out on a gas chromatography workstation (GC-950, Hua'ai Co.) at different heating rates from 2 to 12 K/min. In each experiment, about 0.01 g of sample that had adsorbed acetone vapour was packed in a stainless-steel column whose inner diameter was 0.3 cm and whose packed length was about 0.5 cm. Subsequently, the stainless tube was placed in a reaction furnace, and then heated in the high-purity N_2 flow at a constant flow rate of 30 mL/min. As the sample was heated at different heating rates from 2 to 12 K/min., acetone desorbed gradually. The desorbed acetone was measured by using the GC-950 chromatograph with a flame ionization detector (FID) at the outlet of the stainless reaction tube, and effluent curves were recorded, which were called the TPD curves. According to the experimental TPD curves, the activation energy for desorption of acetone on the sample can be estimated.

3 Results and discussion

3.1 Physical characteristics. Figure 1 (a) (b) and (c) exhibit the scanning electron microscope (SEM) images of the materials prepared in this work. Figure 1(b) shows that the sample MIL-101 had clear octahedral crystals. Figure 1(c) shows the agglomerates of the GrO@MIL-101. Neither the GrO@MIL-101 was similar to the MIL-101 crystal, nor to the GrO. Figure 1(d), (e) and (f) give the transmission electron microscope (TEM) images of the samples. It can be seen from Figure 1(d) that the GrO had a layered structure. For the GrO@MIL-101 composite, it can be observed that the MIL-101 units were embedded in the GrO layers, as shown in Figure 1(f). These pictures show that the GrO and the MIL-101 component were bond together within the composite. It was also observed that the MIL-101 crystals in GrO@MIL-101 composite seemed different from the parental ones. The sizes of the former were smaller than that of the latter. The reason may be that there were additional constraints in the degrees of freedom for the growth of the MIL-101 crystals during the synthesis of the composite caused by presence of the GrO. In other words, during the growth of the MIL-101 crystals in the synthesis, the GrO in the composite exerted distortion force on the crystals, resulting in distorted structures and diminishment of the

CREATED USING THE RSC ARTICLE TEMPLATE (VER. 3.0) - SEE WWW.RSC.ORG/ELECTRONICFILES FOR DETAILS

ARTICLE TYPE www.rsc.org/xxxxxx | XXXXXXXX

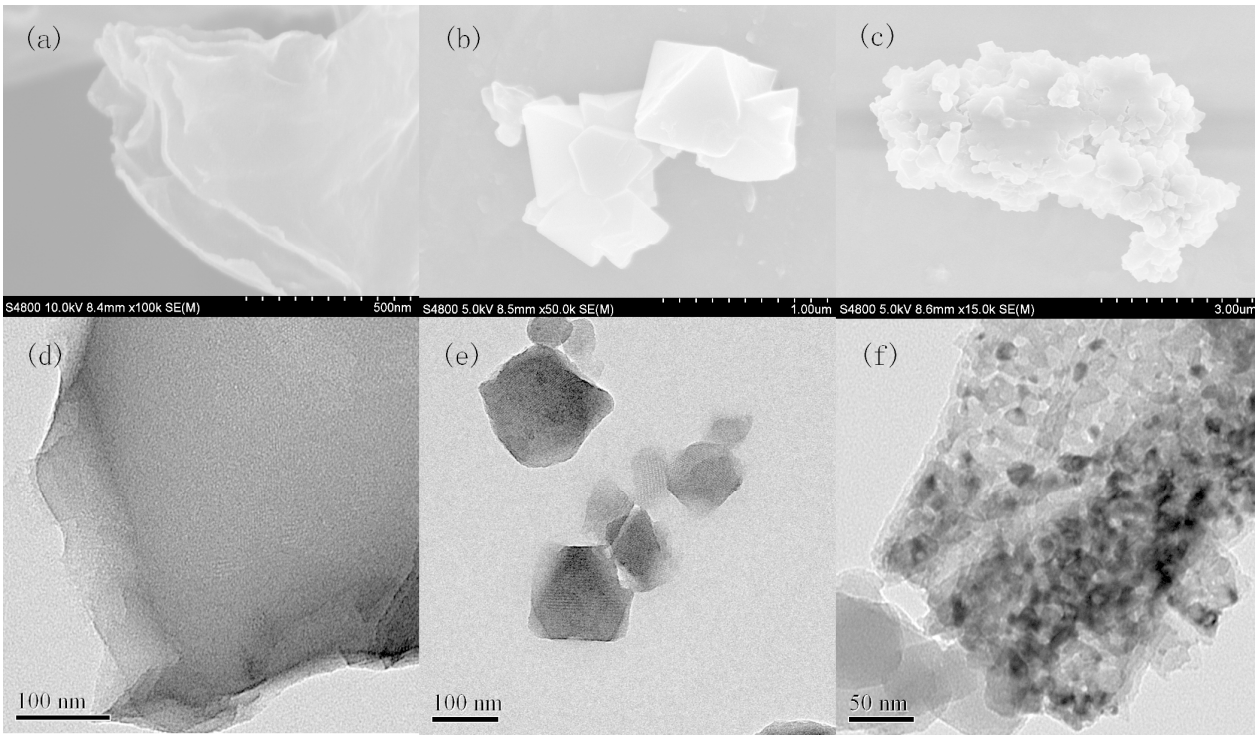

Figure 1. SEM images of (a) GrO, (b) MIL-101 and (c) GrO@MIL-101; TEM images of (d) GrO, (e) MIL-101 and (f) GrO@MIL-101.

crystals. It indicated that the presence of the GrO may have certain influences on the growth of MIL-101 crystals during their formation.

Figure 2 shows the powder X-ray diffraction (XRD) patterns of the GrO, MIL-101, their physical mixture GrO+MIL-101 and the composite GrO@MIL-101 synthesized in this work. The major diffraction pattern of the composite GrO@MIL-101 was nearly the same as that of the MIL-101 previously reported.[13] The reason was that the MIL-101 represents the major component of the composite, and it also suggested that the GrO@MIL-101 preserved the crystalline characters of parental MIL-101. Of course, This phenomenon should only take place if the existence of GrO did not prevented the formation of the MIL-101 crystals in the synthesis of the composite GrO@MIL-101, as mentioned in some other pioneering work.[7] In addition, it was noticed that the diffraction pattern of the composite GrO@MIL-101 was different from that of mixture GrO+MIL-101. The intensity of the peaks for the physical mixture GrO+MIL-101 was obviously weaker compared to the MIL-101, which was possibly because part of MIL-101 crystals in the physical mixture were sheltered by GrO. The GrO is amorphous, and revealed no visible peak in the XRD tested region.

Figure 3 gives the Fourier transform infrared spectroscopy (FTIR) spectra of the five samples such as GrO, the MIL-101, their physical mixture GrO+MIL-101, the composite GrO@MIL-101 and the graphite. It was observed that the spectrum for the GrO was distinct from that for the graphite in that the former exhibited a band at 1112 cm^{-1}, which was assigned to C-O stretching vibrations of the GrO.[16] It was also observed in the spectrum of physical mixture GrO+MIL-101, as expected. However, interestingly, this band disappeared in the spectrum for the GrO@MIL-101. The reason may be that the oxygen functional groups on the GrO layers were bond with the open metal sites of MIL-101 and thus led to the disappearance of this band for GrO. Similar hypothesis had been proposed by Bandosz and coworkers in the case of MOF-GO composite[15, 16]. They reported that oxidation of graphite caused the introduction of oxygen functional groups into the graphene layers, which was helpful in formation of the bonds between the components of graphene layers and MOF units.

Figure 4 shows Raman spectra of four samples such as the GrO, MIL-101, their physical mixture GrO+MIL-101 and the composite GrO@MIL-101. The spectrum of the GrO@MIL-101 preserved the characteristic bands of the MIL-101 as reported elsewhere.[17] The typical features in the spectrum of GrO were the G band at 1593 cm^{-1} and the D band at 1352 cm^{-1}. The remarkable D band in the Raman was an indication of disorder originating from defects of the GrO.[18] The spectrum of GrO@MIL-101 was different from physical mixture of the GrO+MIL-101 in that the characteristic peak intensity of the former was very strong, while that of the later was very weak. The reason may be that a part of MIL-101 crystals in the physical mixture were sheltered by GrO. In addition, it was also observed that there were two small shoulders appeared in the spectrum of the GrO@MIL-101, corresponding to the G band and the D band of the spectrum of GrO, and it confirmed the existence of GrO structure in the

Journal of Materials Chemistry

Dynamic Article Links ►

Cite this: DOI: 10.1039/c0xx00000x

www.rsc.org/materials

ARTICLE TYPE

GrO@MIL-101. However, the existence of GrO layer in GrO@MIL-101 was different from that in the physical mixture as it did not lower the signal intensity for MIL-101 crystallite. Thus, the sandwich-like structure in which layers of MIL-101 crystallites were separated by the layers of GrO was quite possible.

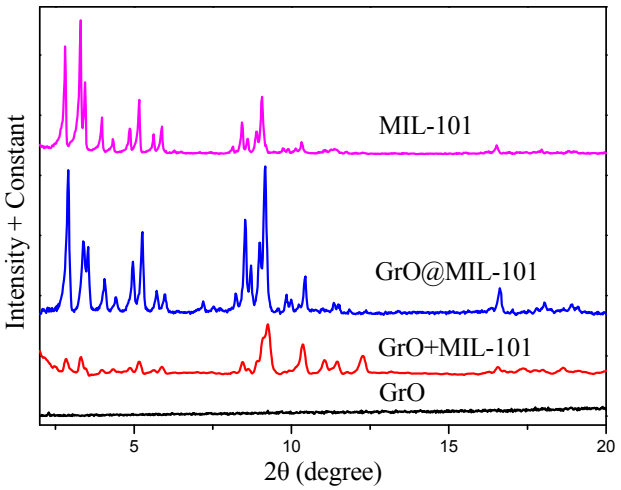

Figure 2. XRD patterns of MIL-101, GrO@MIL-101, GrO+MIL-101 and GrO.

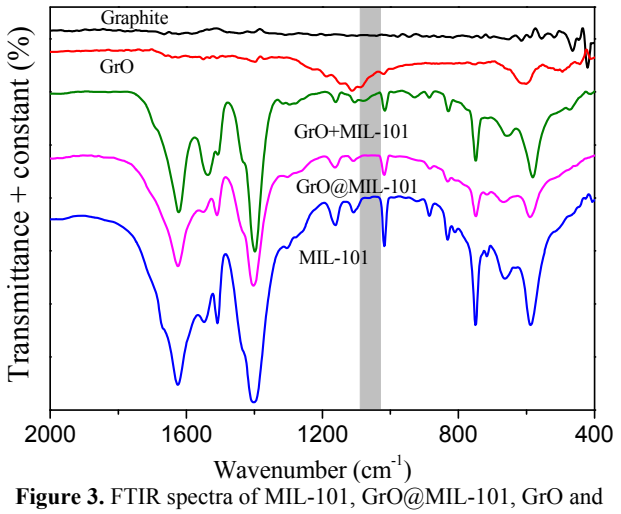

Figure 3. FTIR spectra of MIL-101, GrO@MIL-101, GrO and graphite.

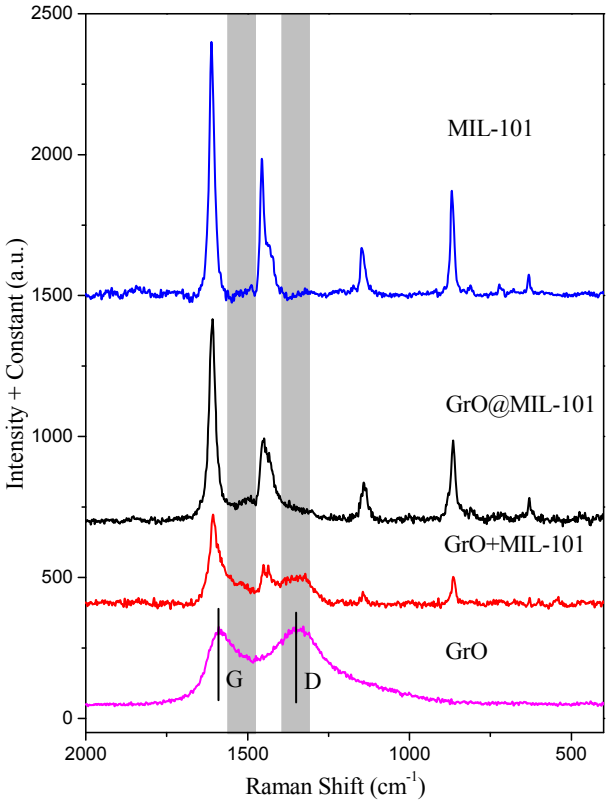

Figure 4. Raman spectra of MIL-101, GrO@MIL-101, GrO+MIL-101 and GrO.

Figure 5 gives N_2 adsorption and desorption isotherms on the GrO@MIL-101 and MIL-101, which are clearly in Type-I profile, the characteristic of microporous structure. It could be seen that isotherm of N_2 on the GrO@MIL-101 was higher than that on the MIL-101, suggesting that specific surface area of the GrO@MIL-101 would be larger. In addition, small hysteresis loop was also observed from the N_2 isotherm on the GrO@MIL-101 as evidence of enhanced mesopores. These mesopores might be new pores between the two "Phases" of MOFs crystals and GrO just as the case of MOF-GO composite as reported elsewhere.[19] Figure 6 gives the pore size distribution curves of the two samples. It was clearly visible that pore size distribution curves of the two samples were similar. The minor difference was in that the pore volume of the GrO@MIL-101 was somewhat higher than the MIL-101, which was in good agreement with the porous structure parameters of two samples in Table 1. Table 1 gives the BET specific areas, Langmuir specific areas and total pore volumes of the two samples. It indicated that the specific surface area and

CREATED USING THE RSC ARTICLE TEMPLATE (VER. 3.0) - SEE WWW.RSC.ORG/ELECTRONICFILES FOR DETAILS

ARTICLE TYPE www.rsc.org/xxxxxx | XXXXXXXX

total pore volume of the GrO@MIL-101 were larger than those of the MIL-101. It could be ascribed to the possibility that the GrO provided new crystallization sites for the MIL-101 crystallites and thus resulted in the enhanced porosity.

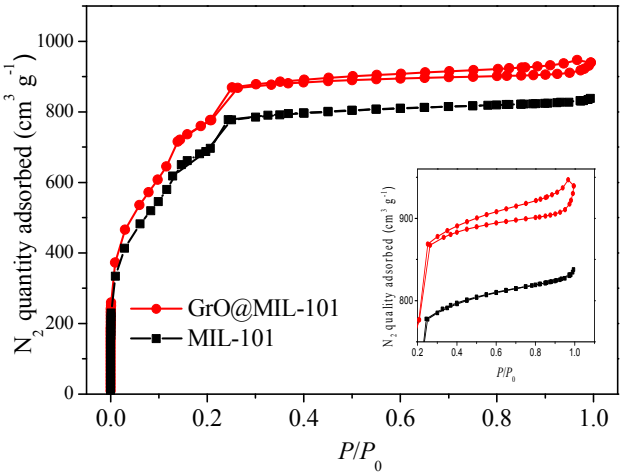

Figure 5. Nitrogen isotherms at 77 K. P/P_0 is the ratio of gas pressure (P) to saturation pressure (P_0=736 mmHg).

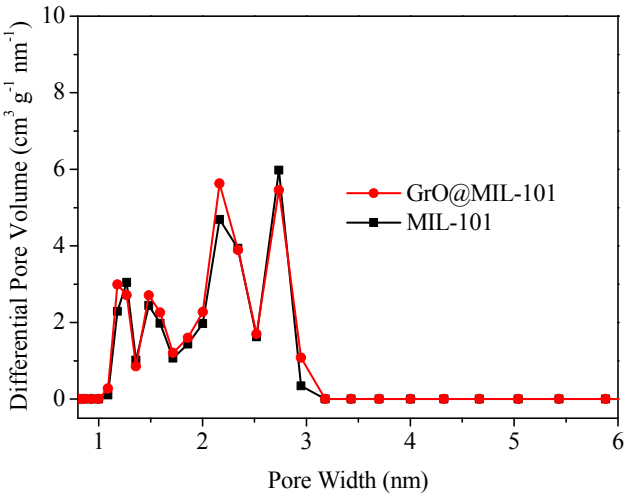

Figure 6. Pore size distribution of GrO@MIL-101 and MIL-101

Table 1. Porous structure parameters of MIL-101 and GrO@MIL-101.

Sample	BET [$m^2 g^{-1}$]	Langmuir [$m^2 g^{-1}$]	Total Pore Volume [$cm^3 g^{-1}$]
MIL-101	2651	3853	1.29
GrO@MIL-101	2928	4254	1.43

The GrO percentage content in the GrO@MIL-101 can be indirectly found out by means of ICP analysis. The results of ICP-AES analysis showed that the Cr percentage contents were separately 17.13% in the MIL-101 and 15.26% in the GrO@MIL-101. The decline of the Cr percentage content in the GrO@MIL-101 mainly resulted from the introduction of the GrO in comparison with the MIL-101. Therefore, the GrO percentage content can be estimated by using following equation.

$$M = 1 - \frac{\omega_1\%}{\omega_2\%} \quad (1)$$

Where M is the GrO content in a unit mass of GrO@MIL-101, ω_1% and ω_2% are Cr percentage contents separately in the MIL-101 and the GrO@MIL-101. M was calculated to be 0.104 from equation (1), indicating the GrO percentage content in the GrO@MIL-101 is 10.9%.

3.2 Adsorption isotherms of acetone. Figure 7 shows the isotherms of acetone on the two samples. It exhibited that the isotherms of acetone became lower with temperature increase, indicating a physisorption between acetone and samples. More interestingly, a significant enhancement of acetone adsorption capacity of the new composite was found in comparison with the parent material MIL-101. Equilibrium amounts adsorbed of acetone on the GrO@MIL-101 were much higher than that on the MIL-101. At 288K, the maximum amount adsorbed of acetone on the GrO@MIL-101 at 161.8 mbar was up to 20.10 mmol g^{-1}, and that on the MIL-101 at 174.7 mbar was 13.92 mmol g^{-1}. The former had an increase of 44.4% in comparison with the latter. This enhancement of acetone adsorption could be attributed to two reasons. One was due to an increase in the BET surface area of the GrO@MIL-101, having an increase of 10.4%. The other reason was due to an increase in the dispersive forces, which could be confirmed with the help of the acetone isotherm based on per unit surface area of the adsorbents. Firstly, the acetone isotherms based on per unit mass of adsorbent were transferred into the acetone isotherms based on per unit surface area, as shown in Figure 8. Then, a comparison of the acetone isotherms of the GrO@MIL-101 and the MIL-101 indicated that the acetone uptakes per unit surface area on the GrO@MIL-101 were much higher than those per unit surface area on the MIL-101. It meant that the surface dispersive forces of the GrO@MIL-101 increased due to introduction of graphene oxide, and thus resulted in the improvement of acetone uptakes per unit surface area of the GrO@MIL-101.

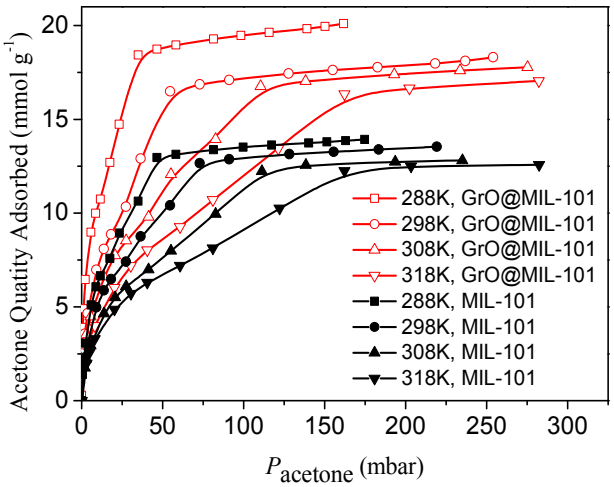

Figure 7. Adsorption isotherms of acetone on the samples at (288 to 318) K.

Journal of Materials Chemistry

Dynamic Article Links ►

Cite this: DOI: 10.1039/c0xx00000x

www.rsc.org/materials

ARTICLE TYPE

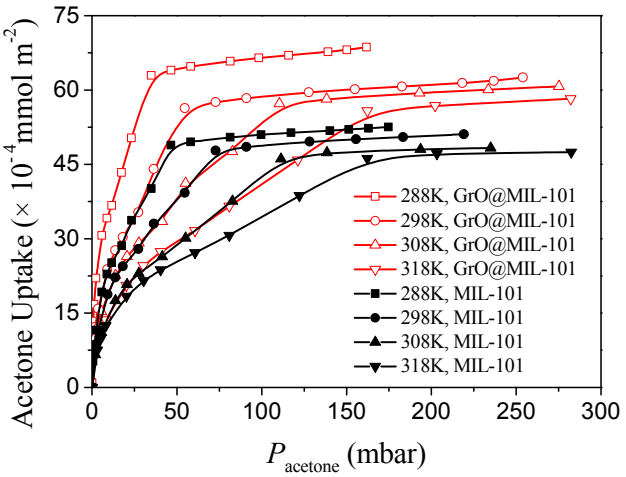

Figure 8. Acetone isotherm on the samples based on unit surface area

Table 2 lists the acetone adsorption capacities of some other adsorbents such as activated carbon fibers, activated carbon, molecular sieves and zeolite. Obviously, the acetone adsorption capacity of GrO@MIL-101 was much higher than those of conventional adsorbents, indicating that the GrO@MIL-101 is a promising adsorbent used for acetone removal.

To describe the adsorption behaviour of acetone, Langmuir-Freundlich (LF) and dual-site Langmuir-Freundlich (DSLF) equations were separately applied to fit the experimental isotherm data of acetone adsorption on the MIL-101 and GrO@MIL-101. Figure 9 gives a comparisons of the experimental data and isotherm equation fits. Table 3 gives the fitting parameters and their correlation coefficients (R^2) which represent the coincidence degree between the isotherm equation fits and experimental data. The correlation coefficients were up to 0.96 for both samples, suggesting that the chosen models can well describe the adsorption behaviour of acetone on both samples.

3.3 Estimation of the isosteric heat of adsorption. Isosteric heat of acetone adsorption can be estimated using Clausius-Clapeyron equation on the acetone isotherms at different temperatures: [20, 21]

$$\frac{dP}{P} = \frac{-\Delta H}{R}\frac{dT}{T^2} \quad (2)$$

$$\ln P = -\Delta H / RT + C \quad (3)$$

Where P is pressure of acetone vapour, and ΔH (kJ·mol^{-1}) is the isosteric heat of acetone adsorption on the samples at specific acetone loading and temperature. Plots $\ln P$ versus 1/T at different amounts adsorbed of acetone, and then the straight lines with slope $-\Delta H / RT$ are yielded. ΔH can be calculated from the slope of the straight lines. Figure 10 shows the dependence of isosteric adsorption heat on the amounts adsorbed of acetone over the samples. It indicated that ΔH of acetone on the GrO@MIL-101 was higher than that on MIL-101.

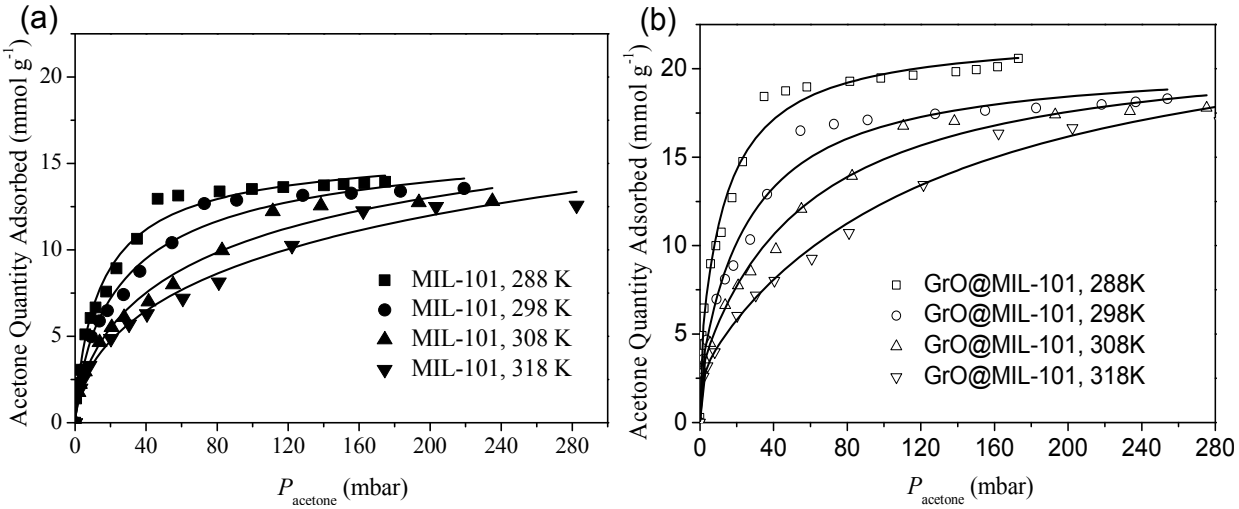

Figure 9. (a) Langmuir-Freundlich equation fitting of acetone adsorption on the MIL-101 (b) Dual-site Langmuir-Freundlich equation fitting of acetone adsorption on the GrO@MIL-101 (points: experimental data; lines: fitting curves).

CREATED USING THE RSC ARTICLE TEMPLATE (VER. 3.0) - SEE WWW.RSC.ORG/ELECTRONICFILES FOR DETAILS

ARTICLE TYPE www.rsc.org/xxxxxx | XXXXXXXX

Table 2. Equilibrium Amount Adsorbed of Acetone on various adsorbents.

Adsorbent	Q_e [mmol g^{-1}]	Temperature [K]	Pressure or Inlet Concentration	Reference
ACF	0.051	298	1000 [ppmv]	[22]
BASF AC	6.2	298	200 [mbar]	[23]
Coconut based AC	2.018	293	200 [ppmv]	[24]
MSPs	2.429	318	8700 [ppmv]	[25]
Si-MSMs-41	2.713	318	8700 [ppmv]	[25]
DAY-zeolite	2.355	293	230 [mbar]	[26]
MIL-101	13.93	288	174.7 [mbar]	present work
GrO@MIL-101	20.58	288	161.8 [mbar]	present work

Table 3. Fitting Parameters of the Langmuir-Freundlich Equations (LF) for MIL-101 and Dual-Site Langmuir-Freundlich Equations (DSLF) for GrO@MIL-101.

Temperature	LF: $Q_t = \frac{Q_{max} b p^{1/n}}{(1+bp^{1/n})}$				DSLF: $Q_t = \frac{Q_{1max} b_1 p^{1/n_1}}{(1+b_1 p^{1/n_1})} + \frac{Q_{2max} b_2 p^{1/n_2}}{(1+b_2 p^{1/n_2})}$						
[K]	Q_{max}	b	n	R^2	Q_{1max}	b_1	n_1	Q_{2max}	b_2	n_2	R^2
288	16.2	0.0990	1.19	0.988	15.2	0.447	1.48	5.81	5.91×10^{-9}	0.165	0.999
298	15.9	0.0721	1.21	0.986	12.9	0.264	1.46	6.20	5.96×10^{-10}	0.172	0.999
308	15.7	0.0386	1.13	0.981	12.0	0.215	1.49	7.09	7.67×10^{-7}	0.296	0.997
318	15.4	0.0350	1.17	0.964	11.1	0.154	1.42	7.75	1.61×10^{-7}	0.298	0.997

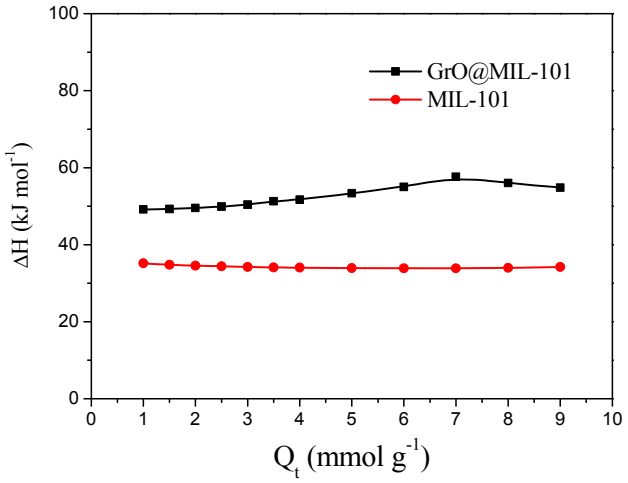

Figure 10. Dependence of isosteric adsorption heat on the amounts adsorbed of acetone over the samples.

3.3 Estimation of the Desorption Activation Energy. Temperature programmed desorption (TPD) technique is a technique of surface analysis. It is usually used to estimate binding energy between an adsorbate and adsorbent surfaces. TPD experiments were conducted to estimate the activation energy of acetone desorption from the materials. Polanyi-Wigner equation was employed to describe the TPD curves: [27, 28]

$$r_d = -\frac{d\theta_A}{dt} = k_0 \theta_A{}^n \exp\left(-\frac{E_d}{RT}\right) \quad (4)$$

Where r_d is the desorption rate (mol s^{-1}), k_0 is a constant that depends on the desorption kinetics (s^{-1}), θ_A is the fractional coverage of adsorbent surface, n is the order of the desorption process, E_d is the desorption activation energy of adsorbate (kJ mol^{-1}), and R is the gas constant (8.314 J K^{-1} mol^{-1}). Assume the desorption process follows first-order kinetics (n=1) and the desorption activation energy of the adsorbate can be calculated by [29]:

$$\ln\left(\frac{RT_p^2}{\beta_H}\right) = \frac{E_d}{RT_p} + \ln\left(\frac{E_d}{k_0}\right) \quad (5)$$

Where β_H is the heating rate (K min^{-1}), T_p is the peak temperature of TPD curves.

Figure 11 (a) shows the TPD spectra of acetone on the GrO@MIL-101 at different heating rates from 2 to 12 K/min. Figure 11 (b) plotted $\ln(RT_p^2/\beta_H)$ versus $1/T_p$, and thus a straight line with the slope E_d/R was available. The slope was calculated to be 7.539 and thus the desorption activation energy of acetone on the GrO@MIL-101 was 62.68 kJ mo^{-1}. In a similar way, the desorption activation energy of acetone on the MIL-101 could also be estimated to be 48.01 kJ mol^{-1}. Obviously, the desorption activation energy of acetone on the GrO@MIL-101 was higher than that on the MIL-101, suggesting that the introduction of GrO sheets into MIL-101 greatly enhanced the interaction of acetone molecules with the surfaces of the GrO@MIL-101.

Journal of Materials Chemistry

Dynamic Article Links ►

Cite this: DOI: 10.1039/c0xx00000x

www.rsc.org/materials

ARTICLE TYPE

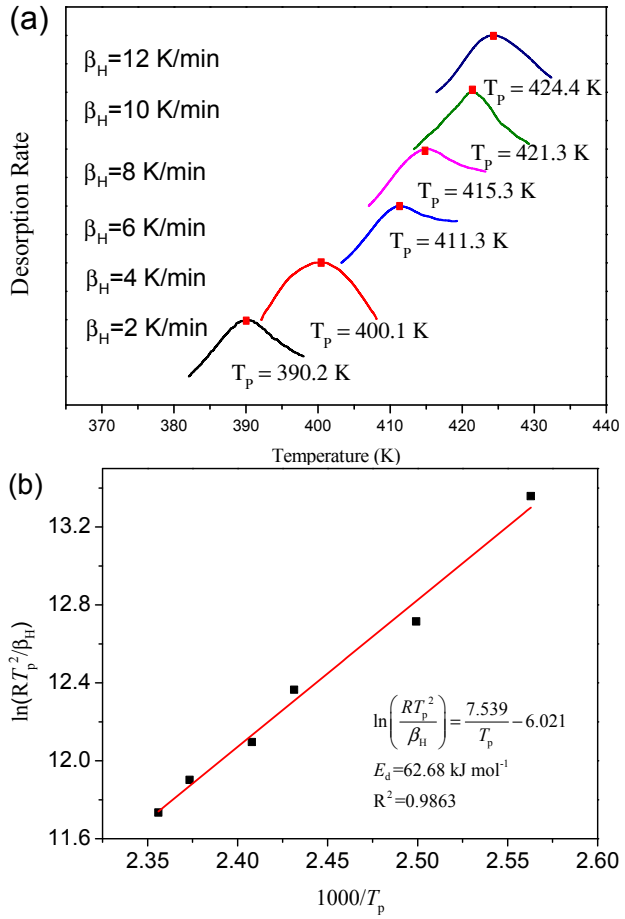

Figure 11. (a) Temperature-programmed desorption (TPD) spectra of acetone on the GrO@MIL-101 at the different heating rates from 2 to 12 K/min (N_2 flow rate: 35 mL min^{-1}); (b) $\ln(RT_p^2/\beta_H)$ versus $1/T_p$ for the estimation of desorption activation energy of acetone on the GrO@MIL-101.

3.4 Multiple Cycles of Acetone Adsorption-Desorption on the samples. In order to examine the reversibility of acetone adsorption on the GrO@MIL-101, the multiple recycle run experiment of acetone adsorption-desorption was performed at 298 K by swinging pressure. In the experiments, adsorption was carried out at (1, 2, 5, 10, 20, 50) mbar separately, and desorption was performed at 0.04 mbar. The multiple adsorption-desorption curve was recorded to evaluate the adsorption-desorption property of the samples.

Figure 12 shows the resulting adsorption-desorption curve from six cycles in 900 min at 298 K. It can be observed that the equilibrium amounts adsorbed of acetone increased with adsorption pressure, and during desorption at 0.04 mbar, the amounts adsorbed of acetone sharply declined to about 1.5 mmol g^{-1} for each of six adsorption-desorption cycles. No more acetone residual could be observed in the next cycles compared to that of the first cycle. The desorption efficiency of acetone could reach 91.3% for the sixth cycles, and the net adsorption capacity was still up to 18.4 mmol g^{-1}. It suggested that the GrO@MIL-101 had excellent reversibility of acetone adsorption. The properties of low accumulation, fast adsorption and desorption and the excellent reversibility made the GrO@MIL-101 a promising candidate for acetone adsorption.

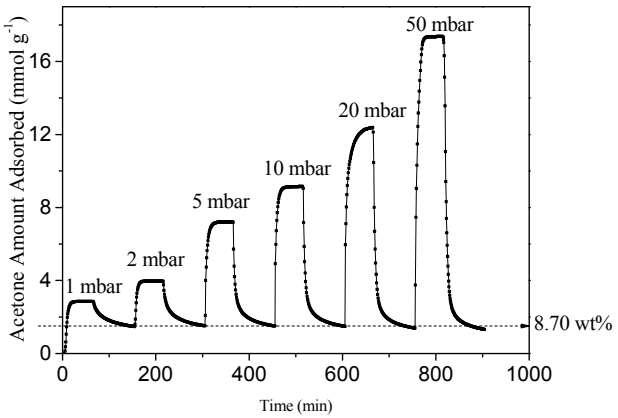

Figure 12. Six consecutive cycles of acetone adsorption-desorption on the GrO@MIL-101 at 298K.

4 Conclusions

Combining the uniqueness of GrO sheets and MIL-101, we synthesized a novel composite GrO@MIL-101 with enhanced adsorption property. The results of characterization confirmed the formation of the well-defined GrO@MIL-101 with higher surface area and pore volume, and the crystal sizes of the MIL-101 in the composite were smaller than that of the parent MIL-101, which may be ascribed to the additional constraints for the growth of the MIL-101 crystals caused by the presence of GrO. The adsorption capacity of the GrO@MIL-101 for acetone was up to 20.10 mmol g^{-1} at 288 K and 161.8 mbar, which was much higher than that of the MIL-101 (13.92 mmol g^{-1}), have an increase of 44.4 %. The enhancement of acetone adsorption could be attributed to the increases in the BET surface area of the GrO@MIL-101 and the dispersive forces due to the introduction of GrO sheets. The isosteric heat of acetone adsorption on the GrO@MIL-101 was higher than that on the MIL-101. TPD results showed that

CREATED USING THE RSC ARTICLE TEMPLATE (VER. 3.0) - SEE WWW.RSC.ORG/ELECTRONICFILES FOR DETAILS

ARTICLE TYPE www.rsc.org/xxxxxx | XXXXXXXX

desorption activation energies of acetone on the GrO@MIL-101 and the MIL-101 were separately 62.68 kJ mol^{-1} and 48.01 kJ mol^{-1}, suggesting that the interaction between the GrO@MIL-101 surfaces and acetone molecules became stronger compared to the MIL-101. The desorption efficiency of acetone on the composite could reach 91.3% for the sixth cycles. It suggested that the GrO@MIL-101 had excellent reversibility of acetone adsorption. The properties of low accumulation, fast adsorption and desorption and the excellent reversibility make the GrO@MIL-101 a promising candidate for adsorption of VOCs such as acetone.

Acknowledgements

This work was supported by National Key Basic Research Program of China (2013CB733506), National Science Fund for Distinguished Young Scholars of China (No.21225616), Fundamental Research Funds for the Central Universities, and National Natural Science Foundation of China (No. 20936001, 21276092).

Notes and references

* *School of Chemistry and Chemical Engineering, South China University of Technology, Guangzhou, 510641, P.R. China. Tel: +86 020 2223 6416; Email: cezhli@scut.edu.cn*

1. L. J. Murray, M. Dinca and J. R. Long, *Chem. Soc. Rev.*, 2009, **38**, 1294-1314.
2. J.-R. Li, R. J. Kuppler and H.-C. Zhou, *Chem. Soc. Rev.*, 2009, **38**, 1477-1504.
3. M. G. Rabbani and H. M. El-Kaderi, *Chemistry of Materials*, 2012, **24**, 1511-1517.
4. W. Zhuang, D. Yuan, D. Liu, C. Zhong, J.-R. Li and H.-C. Zhou, *Chem. Mater.*, 2012, **24**, 18-25.
5. S. T. Meek, J. A. Greathouse and M. D. Allendorf, *Adv. Mater.*, 2011, **23**, 249-267.
6. J. R. Long and O. M. Yaghi, *Chem. Soc. Rev.*, 2009, **38**, 1213-1214.
7. C. Petit and T. J. Bandosz, *Adv. Mater.*, 2009, **21**, 4753-4757.
8. C. Petit, B. Levasseur, B. Mendoza and T. J. Bandosz, *Microporous Mesoporous Mater.*, 2012, **154**, 107-112.
9. C. Petit and T. J. Bandosz, *J. Mater. Chem.*, 2009, **19**, 6521-6528.
10. T. J. Bandosz and C. Petit, *Adsorption-Journal of the International Adsorption Society*, 2011, **17**, 5-16.
11. B. Levasseur, C. Petit and T. J. Bandosz, *ACS Appl. Mat. Interfaces*, 2010, **2**, 3606-3613.
12. C. Petit and T. J. Bandosz, *Adv. Funct. Mater.*, 2011, **21**, 2108-2117.
13. G. Ferey, C. Mellot-Draznieks, C. Serre, F. Millange, J. Dutour, S. Surble and I. Margiolaki, *Science*, 2005, **309**, 2040-2042.
14. W. S. Hummers and R. E. Offeman, *J. Am. Chem. Soc.*, 1958, **80**, 1339-1339.
15. P. Lian, X. Zhu, S. Liang, Z. Li, W. Yang and H. Wang, *Electrochim. Acta*, 2010, **55**, 3909-3914.
16. T. Szabo, O. Berkesi and I. Dekany, *Carbon*, 2005, **43**, 3186-3189.
17. C. M. Granadeiro, A. D. S. Barbosa, P. Silva, F. A. Almeida Paz, V. K. Saini, J. Fires, B. de Castro, S. S. Balula and L. Cunha-Silva, *Applied Catalysis a-General*, 2013, **453**, 316-326.
18. Y. Zhou, Q. Bao, L. A. L. Tang, Y. Zhong and K. P. Loh, *Chemistry of Materials*, 2009, **21**, 2950-2956.
19. M. Seredych, C. Petit, A. V. Tamashausky and T. J. Bandosz, *Carbon*, 2009, **47**, 445-456.
20. J. Shi, Z. Zhao, Q. Xia, Y. Li and Z. Li, *J. Chem. Eng. Data*, 2011, **56**, 3419-3425.
21. Z. Zhao, Z. Li and Y. S. Lin, *Industrial & Engineering Chemistry Research*, 2009, **48**, 10015-10020.
22. C. L. Mangun, R. D. Braatz, J. Economy and A. J. Hall, *Industrial & Engineering Chemistry Research*, 1999, **38**, 3499-3504.
23. L. Gales, A. Mendes and C. Costa, *Carbon*, 2000, **38**, 1083-1088.
24. M.-G. Lee, S.-W. Lee and S.-H. Lee, *Korean J. Chem. Eng.*, 2006, **23**, 773-778.
25. C. Hung, H. Bai and M. Karthik, *Sep. Purif. Technol.*, 2009, **64**, 265-272.
26. D.-G. Lee, J.-H. Kim and C.-H. Lee, *Sep. Purif. Technol.*, 2011, **77**, 312-324.
27. Q. Xia, Z. Li, L. Xiao, Z. Zhang and H. Xi, *J. Hazard. Mater.*, 2010, **179**, 790-794.
28. X. Li, X. Chen and Z. Li, *J. Chem. Eng. Data*, 2010, **55**, 3164-3169.
29. Z. Zhang, S. Huang, S. Xian, H. Xi and Z. Li, *Energy & Fuels*, 2011, **25**, 835-842.

Journal Name Journal of Materials Chemistry A Dynamic Article Links ►

Cite this: DOI: 10.1039/c0xx00000x

www.rsc.org/xxxxxx

ARTICLE TYPE

Graphical Abstract

A novel composite material GrO@MIL-101 was synthesized using a solvothermal synthesis method. The results of characterization confirmed the formation of well-defined GrO@MIL-101 with higher surface area and pore volume compared to the MIL-101, and the crystal size of the MIL-101 in the composite were smaller than that of the parent MIL-101. The acetone adsorption capacity of the GrO@MIL-101 was up to 20.10 mmol g^{-1} at 288K and 161.8 mbar, having an increase of 44.4% in comparison with the MIL-101. The desorption activation energy of acetone on the GrO@MIL-101 were higher than that on the MIL-101, indicating the stronger interaction between acetone molecules and the GrO@MIL-101. Consecutive cycles of acetone adsorption-desorption showed that the desorption efficiency of acetone on the GrO@MIL-101 can reach 91.3%. Acetone adsorption on this composite material was highly reversible.